ACS Macro Letters

Letter

Cite This: ACS Macro Lett. 2018, 7, 1261−1266

pubs.acs.org/macroletters

Probing Membrane Hydration at the Interface of Self-Assembled Peptide Amphiphiles Using Electron Paramagnetic Resonance

Ian R. Smith, Alban H. R. Charlier, Amanda M. Pritzlaff, Alexander Shishlov, Brooke Barnes, Kyle C. Bentz, Charles P. Easterling, Brent S. Sumerlin, Gail E. Fanucci, and Daniel A. Savin*

George & Josephine Butler Polymer Research Laboratory, Center for Macromolecular Science & Engineering, Department of Chemistry, University of Florida, P.O. Box 117200, Gainesville, Florida 32611-7200, United States

Supporting Information

ABSTRACT: The relative hydrophilicity at the interface of a nanoparticle was measured utilizing electron paramagnetic resonance (EPR) spectroscopy. The supramolecular structure was assembled from spin-labeled peptide amphiphiles (PA) derived from *N*-carboxy anhydrides (NCA). Cyanuric chloride, or 2,4,6-trichloro-1,3,5-triazine (TCT), was used as a modular platform to synthesize the spin-labeled, lipid-mimetic macroinitiator used for the ring-opening polymerization of γ-benzyl-L-glutamic acid NCA to produce polyglutamate-*b*-dodecanethiol$_2$. Through static and dynamic light scattering, as well as transmission electron microscopy, PAs with DP of 50 and 17 were shown to assemble into stable nanoparticles with an average hydrodynamic radius of 117 and 84 nm, respectively. Continuous wave EPR spectroscopy revealed that the mobility parameter (h_{-1}/h_0) and $2A_{iso}$ of the nitroxide radical increased with increasing pH, in concert with the deprotonation of the PE side chains and associated helix−coil transition. These results are consistent with an increase in the relative hydration and polarity at the nanoparticle interface, which would be dependent on the secondary structure of the polypeptide. This research suggests that a pH stimulus could be used to facilitate water diffusion through the membrane.

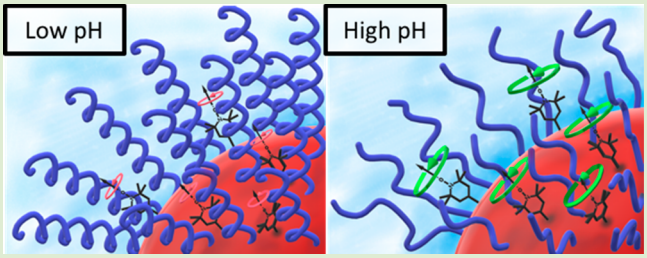

Peptide amphiphiles (PA) are an important class of biomolecules with a variety of applications such as in tissue engineering, regenerative medicine, and drug delivery.[1−5] In general, a PA is composed of a hydrophobic lipid covalently linked to an oligo- or polypeptide headgroup. The polypeptide can be designed to have a specific secondary structure (e.g., random coil, α-helix, β-sheet) as well as possess stimuli responsiveness and bioactivity. Depending on the length and identity of the lipid/polypeptide, it is possible to direct aqueous self-assembly toward the formation of spherical micelles,[6] ribbons,[7] cylinders,[8] or vesicles.[9,10] These nanostructures can be effective drug delivery tools that display a variety of antigens from tailor-made PAs and can internalize within tumor cells.[11]

Although PAs can be tailor-made through solid-phase peptide synthesis, this is a time-consuming process that is limited to short polypeptide lengths and low yields. When specificity is not crucial, it is beneficial to synthesize polypeptides via the ring-opening polymerization (ROP) of *N*-carboxy anhydrides (NCAs). This facile process can be used to polymerize a variety of amino acid NCA derivatives, such as glutamic acid (pK_a = 4.15) and lysine (pK_a = 10.67), in high yield and with high molecular weight.[12,13] For example, Naik et al. and Ray et al. synthesized PAs with an AB_2 structural motif that self-assembled into vesicles.[9,10] For the case of PAs containing polyglutamate (PE) side chains, these ionized at high pH, which led to a transition in secondary structure from an α-helix to extended coil. This α-helix to coil transition is expected to lead to a 0.22 nm increase in radius per monomer unit,[14] which corresponds to a 3.5 nm increase in radius for a polymer with DP = 16. However, they observed a dramatically enhanced pH response, whereby there was a 30 nm increase in hydrodynamic radius that was independent of concentration, with no change in aggregation number across the pH range. It was hypothesized that this enhanced pH response was a result of changing interfacial chain density. It would follow that there would be an associated thinning of the vesicle membrane and associated increase in hydrophilicity at the membrane interface.

Probing noncovalent interactions, such as membrane hydration, and the local environment of complex nanostructures, can be realized through the utility of continuous wave electron paramagnetic resonance (CW EPR) spectroscopy.[15,16] Nitroxide radicals are employed as stable paramagnetic probes that can be covalently linked to proteins, polymers, and nanoparticles.[17−22] CW EPR can readily be used as a qualitative and quantitative tool to obtain information about the local environment up to ca. 2 nm.[23] Although current research elucidates the dynamics and interactions between water and supramolecular nanostructures,[18,21,24,25] we describe

Received: September 20, 2018
Accepted: September 27, 2018
Published: October 1, 2018

DOI: 10.1021/acsmacrolett.8b00728
ACS Macro Lett. 2018, 7, 1261−1266

here the effects of an external stimulus on the local dielectric that can be consistent with changes in interfacial hydration. It is conceivable that a rigid polypeptide in an α-helix conformation would reduce the diffusion of water molecules to the hydrophobic surface of the nanostructure, while an ionized and flexible coil would increase polymer chain interactions with water. For instance, it is well-known that poly(ethylene glycol) improves pharmacokinetics and acts as a steric stabilizer to reduce adverse cellular interactions; however, it also reduces the bioactivity of the attached drug/protein.[26] Through course-grained molecular dynamics simulations, Srinivas et al. studied the activity of a transmembrane channel protein embedded in a polymer vesicle.[27] The authors showed that increased length and rigidity of polymer chains in the corona reduced diffusion of water to the surface of the bilayer, thereby affecting the function of the protein. Furthermore, EPR experiments have shown that water dynamics directly affect protein folding and function within the protein apoMb.[21] We believe that increased hydration at the interface of a vesicle bilayer has strong implications toward increased activity of biomolecules, which could potentially be used as a pH-dependent gating mechanism for drug delivery.

To investigate the enhanced pH response observed by Ray et al., we incorporated the nitroxide radical, 2,2,6,6-tetramethylpiperidine-1-oxyl (TEMPO), at the hydrophilic/hydrophobic interface of a PA nanostructure. The benefit of our synthetic approach is the use of 2,4,6-trichloro-1,3,5-triazine (TCT) as a platform for conjugation. Through chemoselective nucleophilic aromatic substitution, the three chlorine atoms on TCT can be sequentially displaced with various functionalities (Scheme S1).[28] TCT has been well studied over the decades as a versatile molecule used as a modular platform for the synthesis of biologically active agents,[29,30] dendrimers,[31,32] and multifunctional polymers.[33−35] Current literature lacks a feasible synthetic approach for PAs that can be performed without a peptide synthesizer, and TCT is the ideal modular platform that fulfills this need. In this study, TCT was utilized as a trisubstituted core molecule for the synthesis of the lipid-mimetic, EPR spin-labeled macroinitiator **4** (Scheme 1) that was used for the

Scheme 1. Synthesis of the Lipid Mimetic and EPR Spin-Labeled Macroinitiator for ROP of NCAs

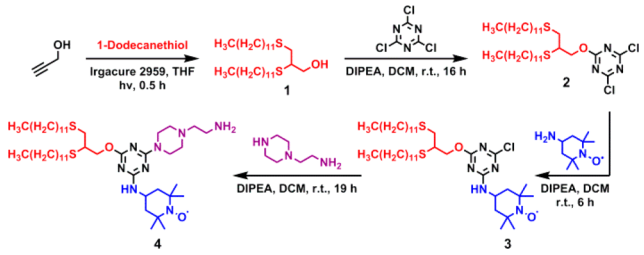

ROP of the γ-benzyl-L-glutamic acid NCA (BLG-NCA) monomer. The particular amino acid can be exchanged for any NCA derivative, while the spin-label is completely interchangeable with other nitroxide radicals. The only limitation is that it must contain a nucleophile for conjugation. After deprotection of the polypeptide, we studied the aqueous self-assembly behavior and pH-responsive effects of the nanoparticles.

First, the lipid-mimetic intermediate **1** was synthesized by the radical-mediated thiol−yne reaction between 1-dodecanethiol and propargyl alcohol (Scheme 1). After purification, **1** was isolated in 84% yield. Second, **2** was prepared by mixing **1** with a slight excess of TCT and DIPEA and was produced in 66% yield after purification. Third, 4-amino-TEMPO was reacted with **2** at room temperature to produce the EPR spin-labeled intermediate **3** in 77% yield after purification. ESI mass spectrometry (ESI-MS) (Figure S4) identified both protiated and sodiated ions related to **3** at m/z 743 and 765, respectively, as well as two peaks at m/z 443 and 394. The sodiated adduct displayed an isotope pattern that suggests the presence of one chlorine atom, thus confirming the successful formation of **3**. In terms of installing a primary amine for initiation of the NCA ROP, it has been previously shown that the nucleophilicity of a cyclic secondary amine is ca. 20 times more reactive than the primary amine in aminomethylpiperidine.[36,37] Due to this, aminoethylpiperazine was chosen to react with the monochlorotriazine **3**, which yielded the final product **4** in 70% yield. LC-MS results identified six major ion contributors (Table S1), which were isolated and fragmented for purity analysis. The two ions at m/z 836 and 837 corresponded to the single and double protonation states, while the ions at m/z 443 and 394 were confirmed to be fragments of m/z 836. Considering these fragments were also present after **3** was ionized, the most likely cause is either the decomposition of the nitroxide radical or fragmentation at the 2-, 4-, or 6-position of the 1,3,5-triazine ring.[38−42] The combined sample percentage of these ions contributed to 88.1% sample purity.

The polymerization of NCAs can be initiated by a variety of nucleophiles and bases. There are two mechanisms of ROP, which are dependent on the strength of bases present in solution. For our purposes, it was important that macroinitiator **4** possess high initiation efficiency for NCA polymerization, with no appreciable side reactions from the nitroxide radical and residual impurities. Nitroxide radicals are known to be stable at room temperature, yet become effective radical trapping agents at elevated temperatures.[43] Therefore, we did not foresee adverse side reactions caused by the nitroxide radical.

Macroinitiator **4** was used to initiate ROP of BLG-NCA to synthesize polyglutamate with a degree of polymerization (DP) of 50 (PE_{50}) or 17 (PE_{17}). Aliquots were periodically taken from the reaction solution and analyzed by gel permeation chromatography (GPC) for molecular weight analysis (Tables S4−S6), and Fourier-transform infrared (FTIR) spectroscopy was used to determine monomer conversion. The polymerization of PE_{17} followed pseudo-first-order kinetics as shown by the linear trend of $\ln(M_0/M)$ versus time (Figure S16). The GPC traces plotted on the inset of the figure provide a good visualization of increasing molecular weight with polymerization time. More importantly, the polymer elution curve remained unimodal throughout the polymerization, thereby indicating that only macroinitiator **4** initiated polymerization of the NCA.

In Figure S16, the number-average molecular weight (M_n) and molar mass dispersity ($Đ$) for the synthesis of PE_{17} were plotted as a function of monomer conversion. The linear increase in M_n with conversion and a near constant dispersity further support control of the polymerization kinetics. The polymer had a final M_n and $Đ$ of 4610 g/mol (which corresponds to a DP of 17) and 1.13, respectively. To better understand the kinetics of the polymerization, monomer conversion was monitored using FTIR spectroscopy. It was observed that 46% of the monomer was consumed after 2.5

DOI: 10.1021/acsmacrolett.8b00728
ACS Macro Lett. 2018, 7, 1261−1266

min (Figure S16). As the polymerization progressed, the consumption of monomer was linearly correlated to polymerization time and then plateaued after ca. 91% monomer consumption.

The radius of gyration (R_g) and hydrodynamic radius (R_h) of the deprotected block polymer assemblies were determined using static and dynamic light scattering. Samples were prepared at 0.05, 0.1, 0.25, and 0.5 wt % concentration from pH 5−10. Precipitation occurred below pH 5, thus this range was excluded from further experiments and characterization. As shown in Figure 1A, the size of the assemblies formed from

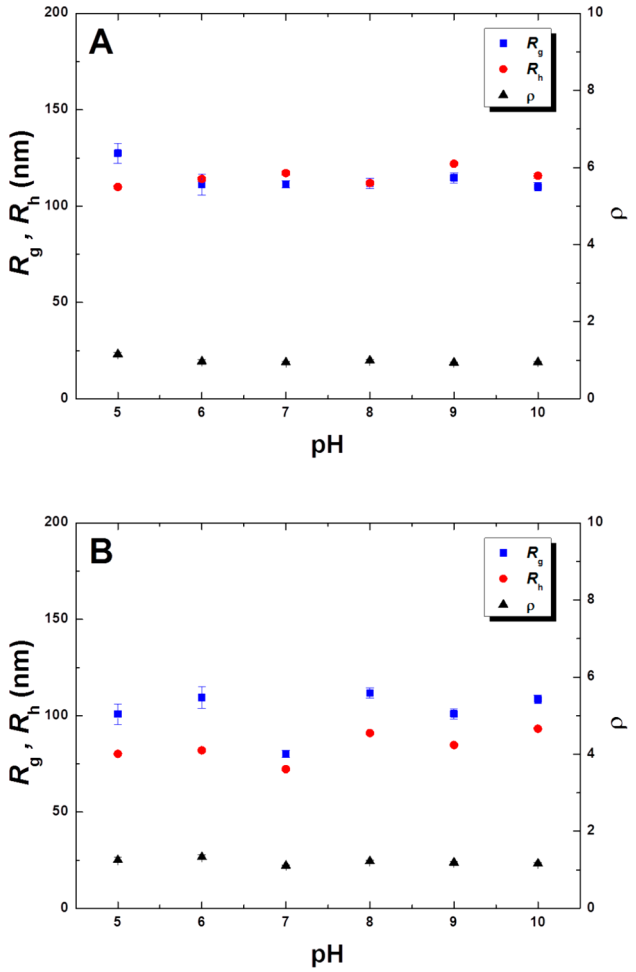

Figure 1. Static and dynamic light-scattering data of the radius of gyration (R_g, ■), hydrodynamic radius (R_h, ●), and ρ (▲) plotted as a function of pH for a 0.1 wt % solution made from polymers with a DP of (A) 50 and (B) 17. Error bars are obtained from the standard deviation.

PE_{50} was invariant with pH, possessing an average R_g, R_h, and ρ of 116 nm, 117 nm, and 0.99, respectively. The radii of these nanoparticles were also shown to be invariant at 0.25 wt %. At the low concentration (0.05 wt %) the R_h increased by 12 nm with increasing pH. At ten times that concentration (0.5 wt %), the R_h fluctuated indiscriminately from the pH of the solution, yet showed an overall increase in size by ca. 20 nm (Figure S17). With the exception of the most concentrated sample, the size of the assemblies showed only slight fluctuations in size. Similar results were found for the assemblies formed from PE_{17}, which possessed an average R_g, R_h, and ρ of 102 nm, 84 nm, and 1.2, respectively (Figure 1B). These results suggest that the nanoparticles were stable over the studied pH range. We did not explicitly see a size increase from the α-helix to coil transition with increasing pH, but circular dichroism showed that there was still appreciable helical character at pH 5 (Figure S20). Protonation of the tertiary amine in the piperazine may also have a potential effect on the pH response. Light-scattering measurements were in agreement with the size of the nanoparticles determined by transmission electron microscopy (Figure S21).

A TEMPO moiety was utilized as the nitroxide spin label to probe the changes in the local environment at the interface of the nanostructure as the pH was modulated. Analysis of the CW EPR line shapes provides information on the relative rotational diffusion (i.e., mobility) of the nitroxide radical. The observed spectra are reflective of fast motional averaging, where the splitting between transitions reports on the relative hydrophilicity of the local environment. The intensity-normalized (h_o) CW EPR spectra for both PE_{17} and PE_{50} are plotted in Figure 2. It can be seen that the high-field (h_{-1})

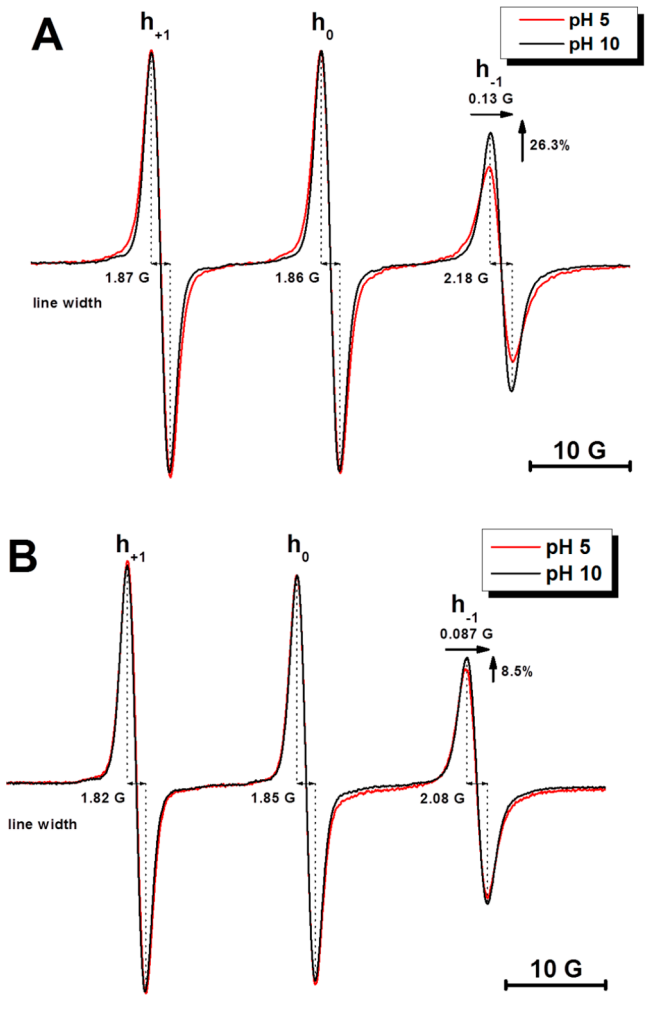

Figure 2. 100 G CW EPR spectra for 0.1 wt % solution of the polymer with a DP of (A) 50 and (B) 17. The peak−peak line widths for the low (h_{+1}), zero (h_0), and high (h_{-1}) field transitions are reported as averages from the pH range studied. Data are plotted as intensity normalized to the h_0 transition. The arrow above the h_{-1} transition demonstrates the magnitude of the change in peak splitting, commensurate with changes in $2A_{iso}$ and hydrophilicity between pH 5−10.

DOI: 10.1021/acsmacrolett.8b00728
ACS Macro Lett. 2018, 7, 1261−1266

transition possessed dampened signal intensity and broader line widths compared to that of the central (h_0) and low-field (h_{+1}) transitions. Furthermore, the h_{-1} intensity increased as the pH increased. This effect was more pronounced in PE_{50} (26%) compared to PE_{17} (8%).

The spectra in Figure 2 are reflective of a TEMPO moiety attached to a polymer with fast-limit mobility in the nanoscale time regime.[17] When TEMPO is freely diffusing in solution, an isotropic line shape is observed where each transition would have the same intensity and width. Therefore, the reduced h_{-1} transition indicates that TEMPO was incorporated into the aggregate and that the nitroxide radical possessed reduced rotational diffusion. This was an expected result, considering that TCT acted as a tether for three (macro)molecules connected at a single junction point. TCT increased the overall rigidity of the PA and introduced a kink into the molecular motif. It has been previously reported that kinks can disrupt the formation of organogels,[44] β-sheets,[45] and nanofibers.[46] Therefore, increased rigidity and the introduction of a kink could have disrupted the mechanism of the pH-enhanced response as previously reported by Ray et al.

The mobility and hydrophilicity parameters (h_{-1}/h_0 and $2A_{iso}$, respectively) are plotted in Figure 3. Both parameters

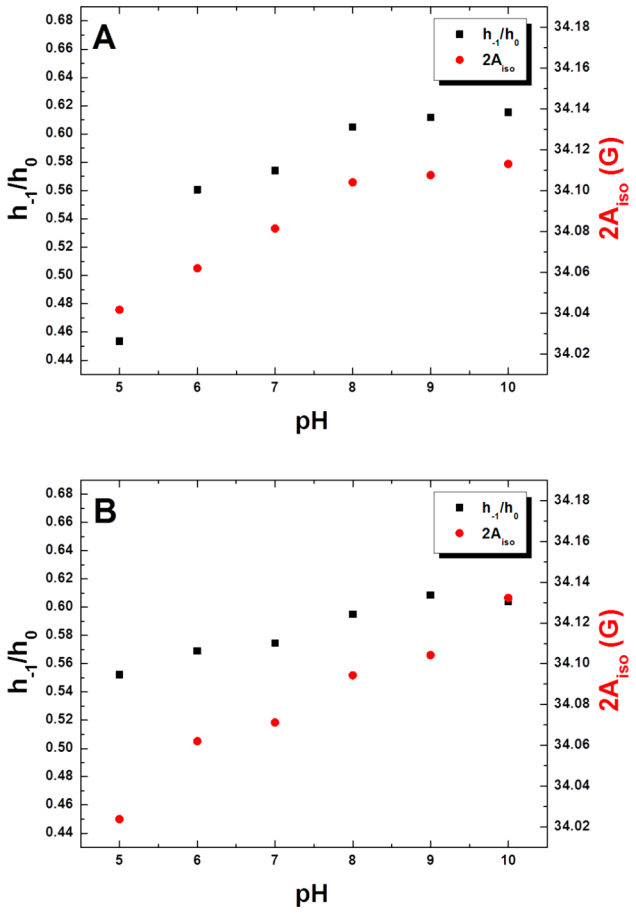

Figure 3. EPR data for 0.1 wt % solution of the polymer with a DP of (A) 50 and (B) 17.

increased with increasing pH. These data indicate that the nitroxyl radical possessed a larger range of rotational motion at high pH, which could manifest from either the total rate of motion and/or angular fluctuations. Similar to previous differences noted above, there is a more pronounced change in the h_{-1}/h_0 in PE_{50} compared to PE_{17}. These differences arise from a more restricted mobility at pH 5 for PE_{50}. A mobility parameter of 1 would correspond to a freely diffusing TEMPO molecule. The hyperfine interaction in the nitroxide radical (i.e., the splitting of the three transitions) is sensitive to the polarity of the environment. This can be measured by the $2A_{iso}$ (measured from the zero of h_{+1} to the zero of h_{-1}, Figures S22−S23), where larger values correlate with a greater hydrophilicity.[47,48]

The EPR findings are consistent with our original hypothesis, where deprotonation of the PE side chains results in a decrease in interfacial curvature due to electrostatic repulsions between the γ-acids on the side chains. Potentially, this would lead to an environment that is more favorable for water diffusion to the interface of the assembly and increased radical mobility. Thus, with PE in the charged, coiled state, we believe that water was able to diffuse more freely to the interface of the nanostructure, thereby relieving conformational constraints and increasing mobility of the nitroxide radical. The increase in hydration at the surface of the membrane could potentially be utilized as a gating mechanism for protein function, which is dependent on the pH-responsive transition in polypeptide secondary structure.

In summary, X-band CW EPR spectroscopy was used as a local probe of mobility and polarity at the interface of self-assembled, pH-responsive PAs. This underutilized probe demonstrated that both probe mobility and local polarity increased with increasing deprotonation of the peptide. These results allude to a potential increase in local hydration at the interface, but future studies are necessary to completely elucidate this relationship. Increased hydration at the nanoparticle interface could potentially be used as a pH-dependent gating mechanism for embedded proteins or other drug delivery applications. Finally, our synthetic strategy offers a modular approach for the conjugation of spin labels and additional functional groups to TCT.

■ ASSOCIATED CONTENT

Supporting Information

The Supporting Information is available free of charge on the ACS Publications website at DOI: 10.1021/acsmacrolett.8b00728.

Experimental materials and methods, reaction schemes, and results for transition electron microscopy, circular dichroism, and mass spectrometry (PDF)

■ AUTHOR INFORMATION

Corresponding Author

*E-mail: savin@chem.ufl.edu.

ORCID

Brent S. Sumerlin: 0000-0001-5749-5444

Daniel A. Savin: 0000-0002-9235-517X

Author Contributions

The manuscript was written through contributions of all authors. All authors have given approval to the final version of the manuscript.

Notes

The authors declare no competing financial interest.

DOI: 10.1021/acsmacrolett.8b00728
ACS Macro Lett. 2018, 7, 1261−1266

■ ACKNOWLEDGMENTS

We thank NSF CHE 1213840/1539347 (D.A.S.), NSF MCB-1715384 (G.E.F.), NSF DMR-1606410 (B.S.S.), NIH 1S10-RR031603-01 (EPR Instrumentation), and NIH S10 OD021758-01A1 (Mass Spectrometry Instrumentation) for funding. We would like to thank Dr. Michael Harris and his group for their assistance with the circular dichroism spectroscopy instrument, as well as Laura Bailey and the Mass Spectrometry Research and Education Center at the University of Florida.

■ REFERENCES

(1) Biesalski, M.; Tu, R.; Tirrell, M. V. Polymerized Vesicles Containing Molecular Recognition Sites. *Langmuir* **2005**, *21*, 5663−5666.
(2) Cui, H.; Webber, M. J.; Stupp, S. I. Self-Assembly of Peptide Amphiphiles: From Molecules to Nanostructures to Biomaterials. *Biopolymers* **2010**, *94* (1), 1−18.
(3) Jiao, D.; Geng, J.; Loh, X. J.; Das, D.; Lee, T.-C.; Scherman, O. A. Supramolecular Peptide Amphiphile Vesicles through Host-Guest Complexation. *Angew. Chem., Int. Ed.* **2012**, *51* (38), 9633−9637.
(4) Chen, Y.; Gan, H. X.; Tong, Y. W. PH-Controlled Hierarchical Self-Assembly of Peptide Amphiphile. *Macromolecules* **2015**, *48* (8), 2647−2653.
(5) Wan, Y.; Wang, Z.; Sun, J.; Li, Z. Extremely Stable Supramolecular Hydrogels Assembled from Nonionic Peptide Amphiphiles. *Langmuir* **2016**, *32*, 7512−7518.
(6) Gore, T.; Dori, Y.; Talmon, Y.; Tirrell, M.; Bianco-Peled, H. Self-Assembly of Model Collagen Peptide Amphiphiles. *Langmuir* **2001**, *17*, 5352−5360.
(7) Pashuck, E. T.; Stupp, S. I. Direct Observation of Morphological Tranformation from Twisted Ribbons into Helical Ribbons. *J. Am. Chem. Soc.* **2010**, *132* (26), 8819−8821.
(8) Ziserman, L.; Lee, H.-Y.; Raghavan, S. R.; Mor, A.; Danino, D. Unraveling the Mechanism of Nanotube Formation by Chiral Self-Assembly of Amphiphiles. *J. Am. Chem. Soc.* **2011**, *133* (8), 2511−2517.
(9) Ray, J. G.; Ly, J. T.; Savin, D. A. Peptide-Based Lipid Mimetics with Tunable Core Properties via Thiol−alkyne Chemistry. *Polym. Chem.* **2011**, *2* (7), 1536.
(10) Naik, S. S.; Chan, J. W.; Comer, C.; Hoyle, C. E.; Savin, D. A. Thiol-Yne "click" Chemistry as a Route to Functional Lipid Mimetics. *Polym. Chem.* **2011**, *2*, 303−305.
(11) Tanaka, A.; Fukuoka, Y.; Morimoto, Y.; Honjo, T.; Koda, D.; Goto, M.; Maruyama, T. Cancer Cell Death Induced by the Intracellular Self-Assembly of an Enzyme-Responsive Supramolecular Gelator. *J. Am. Chem. Soc.* **2015**, *137*, 770−775.
(12) Naik, S. S.; Ray, J. G.; Savin, D. A. Temperature-and PH-Responsive Self-Assembly of Poly(Propylene Oxide)-b-Poly(Lysine) Block Copolymers in Aqueous Solution. *Langmuir* **2011**, *27*, 7231−7240.
(13) Ray, J. G.; Naik, S. S.; Hoff, E. A.; Johnson, A. J.; Ly, J. T.; Easterling, C. P.; Patton, D. L.; Savin, D. A. Stimuli-Responsive Peptide-Based ABA-Triblock Copolymers: Unique Morphology Transitions With PH. *Macromol. Rapid Commun.* **2012**, *33* (9), 819−826.
(14) Ray, J. G.; Johnson, A. J.; Savin, D. A. Self-Assembly and Responsiveness of Polypeptide-Based Block Copolymers: How "Smart" Behavior and Topological Complexity Yield Unique Assembly in Aqueous Media. *J. Polym. Sci., Part B: Polym. Phys.* **2013**, *51* (7), 508−523.
(15) Naveed, K.-R.; Wang, L.; Yu, H.; Summe Ullah, R.; Haroon, M.; Fahad, S.; Li, J.; Elshaarani, T.; Ullah Khan, R.; Nazir, A. Recent Progress in the Electron Paramagnetic Resonance Study of Polymers. *Polym. Chem.* **2018**, *9*, 3306−3335.
(16) Kurzbach, D.; Junk, M. J. N.; Hinderberger, D. Nanoscale Inhomogeneities in Thermoresponsive Polymers. *Macromol. Rapid Commun.* **2013**, *34* (2), 119−134.
(17) Esquiaqui, J. M.; Sherman, E. M.; Ionescu, S. A.; Ye, J.-D.; Fanucci, G. E. Characterizing the Dynamics of the Leader−Linker Interaction in the Glycine Riboswitch with Site-Directed Spin Labeling. *Biochemistry* **2014**, *53*, 3526−3528.
(18) Ortony, J. H.; Qiao, B.; Newcomb, C. J.; Keller, T. J.; Palmer, L. C.; Deiss-Yehiely, E.; Olvera de la Cruz, M.; Han, S.; Stupp, S. I. Water Dynamics from the Surface to the Interior of a Supramolecular Nanostructure. *J. Am. Chem. Soc.* **2017**, *139*, 8915−8921.
(19) Ortony, J. H.; Newcomb, C. J.; Matson, J. B.; Palmer, L. C.; Doan, P. E.; Hoffman, B. M.; Stupp, S. I. Internal Dynamics of a Supramolecular Nanofiber. *Nat. Mater.* **2014**, *13* (8), 812−816.
(20) Bull, S. R.; Guler, M. O.; Bras, R. E.; Meade, T. J.; Stupp, S. I. Self-Assembled Peptide Amphiphile Nanofibers Conjugated to MRI Contrast Agents. *Nano Lett.* **2005**, *5* (1), 1−4.
(21) Armstrong, B. D.; Choi, J.; Opez, C. L.; Wesener, D. A.; Hubbell, W.; Cavagnero, S.; Han, S. Site-Specific Hydration Dynamics in the Nonpolar Core of a Molten Globule by Dynamic Nuclear Polarization of Water. *J. Am. Chem. Soc.* **2011**, *133*, 5987−5995.
(22) Mccarney, E. R.; Armstrong, B. D.; Kausik, R.; Han, S. Dynamic Nuclear Polarization Enhanced Nuclear Magnetic Resonance and Electron Spin Resonance Studies of Hydration and Local Water Dynamics in Micelle and Vesicle Assemblies. *Langmuir* **2008**, *24*, 10062−10072.
(23) Armstrong, B. D.; Han, S. Overhauser Dynamic Nuclear Polarization To Study Local Water Dynamics. *J. Am. Chem. Soc.* **2009**, *131*, 4641−4647.
(24) Kurzbach, D.; Hassouneh, W.; Mcdaniel, J. R.; Jaumann, E. A.; Chilkoti, A.; Hinderberger, D. Hydration Layer Coupling and Cooperativity in Phase Behavior of Stimulus Responsive Peptide Polymers. *J. Am. Chem. Soc.* **2013**, *135*, 11299−11308.
(25) Widder, K.; Macewan, S. R.; Garanger, E.; Núnez, V.; Lecommandoux, S.; Chilkoti, A.; Hinderberger, D. Characterisation of Hydration and Nanophase Separation during the Temperature Response in Hydrophobic/Hydrophilic Elastin-like Polypeptide (ELP) Diblock Copolymers. *Soft Matter* **2017**, *13*, 1816−1822.
(26) Harris, J. M.; Chess, R. B. Effect of Pegylation on Pharmaceuticals. *Nat. Rev. Drug Discovery* **2003**, *2* (3), 214−221.
(27) Srinivas, G.; Discher, D. E.; Klein, M. L. Key Roles for Chain Flexibility in Block Copolymer Membranes That Contain Pores or Make Tubes. *Nano Lett.* **2005**, *5* (12), 2343−2349.
(28) Blotny, G. Recent Applications of 2,4,6-Trichloro-1,3,5-Triazine and Its Derivatives in Organic Synthesis. *Tetrahedron* **2006**, *62* (41), 9507−9522.
(29) Li, H.; Zhou, H.; Krieger, S.; Parry, J. J.; Whittenberg, J. J.; Desai, A. V.; Rogers, B. E.; Kenis, P. J. A.; Reichert, D. E. Triazine-Based Tool Box for Developing Peptidic PET Imaging Probes: Syntheses, Microfluidic Radiolabeling, and Structure− Activity Evaluation. *Bioconjugate Chem.* **2014**, *25*, 761−772.
(30) Banjanac, K.; Mihailović, M.; Prlainović, N.; Stojanović, M.; Carević, M.; Marinković, A.; Bezbradica, D. Cyanuric Chloride Functionalized Silica Nanoparticles for Covalent Immobilization of Lipase. *J. Chem. Technol. Biotechnol.* **2016**, *91* (2), 439−448.
(31) Simanek, E. E.; Abdou, H.; Lalwani, S.; Lim, J.; Mintzer, M.; Venditto, V. J.; Vittur, B. The 8 Year Thicket of Triazine Dendrimers: Strategies, Targets and Applications. *Proc. R. Soc. London, Ser. A* **2010**, *466*, 1445−1468.
(32) Zong, H.; Thomas, T. P.; Lee, K.-H.; Desai, A. M.; Li, M.-H.; Kotlyar, A.; Zhang, Y.; Leroueil, P. R.; Gam, J. J.; Banaszak Holl, M. M.; Baker, J. R. Bifunctional PAMAM Dendrimer Conjugates of Folic Acid and Methotrexate with Defined Ratio. *Biomacromolecules* **2012**, *13*, 982−991.
(33) Figg, C. A.; Kubo, T.; Sumerlin, B. S. Efficient and Chemoselective Synthesis of ω,ω-Heterodifunctional Polymers. *ACS Macro Lett.* **2015**, *4* (10), 1114−1118.

DOI: 10.1021/acsmacrolett.8b00728
ACS Macro Lett. 2018, 7, 1261−1266

(34) Kubo, T.; Figg, C. A.; Swartz, J. L.; Brooks, W. L. A.; Sumerlin, B. S. Multifunctional Homopolymers: Postpolymerization Modification via Sequential Nucleophilic Aromatic Substitution. *Macromolecules* **2016**, *49* (6), 2077−2084.
(35) Kubo, T.; Bentz, K. C.; Powell, K. C.; Figg, C. A.; Swartz, J. L.; Tansky, M.; Chauhan, A.; Savin, D. A.; Sumerlin, B. S. Modular and Rapid Access to Amphiphilic Homopolymers via Successive Chemoselective Post-Polymerization Modification. *Polym. Chem.* **2017**, *8*, 6028−6032.
(36) Moreno, K. X.; Simanek, E. E. Identification of Diamine Linkers with Differing Reactivity and Their Application in the Synthesis of Melamine Dendrimers. *Tetrahedron Lett.* **2008**, *49*, 1152−1154.
(37) Steffensen, M. B.; Simanek, E. E. Chemoselective Building Blocks for Dendrimers from Relative Reactivity Data. *Org. Lett.* **2003**, *5* (13), 2359−2361.
(38) Smith, C. D.; Bartley, J. P.; Bottle, S. E.; Micallef, A. S.; Reid, D. A. Electrospray Ionization Mass Spectrometry of Stable Nitroxide Free Radicals and Two Isoindoline Nitroxide Dimers. *J. Mass Spectrom.* **2000**, *35* (5), 607−611.
(39) Marshall, D. L.; Christian, M. L.; Gryn 'ova, G.; Coote, M. L.; Barker, P. J.; Blanksby, S. J. Oxidation of 4-Substituted TEMPO Derivatives Reveals Modifications at the 1-and 4-Positions. *Org. Biomol. Chem.* **2011**, *9*, 4936−4947.
(40) Niessen, W. M. A. Group-Specific Fragmentation of Pesticides and Related Compounds in Liquid Chromatography-Tandem Mass Spectrometry. *J. Chromatogr. A* **2010**, *1217*, 4061−4070.
(41) Ramesh, M.; Raju, B.; George, M.; Srinivas, K.; Jayathirtha Rao, V.; Bhanuprakash, K.; Srinivas, R. The ESI CAD Fragmentations of Protonated 2,4,6-Tris(Benzylamino)- and Tris(Benzyloxy)-1,3,5-Triazines Involve Benzyl-Benzyl Interactions: A DFT Study. *J. Mass Spectrom.* **2012**, *47* (7), 860−868.
(42) Garver, J. M.; Yang, Z.; Kato, S.; Wren, S. W.; Vogelhuber, K. M.; Lineberger, W. C.; Bierbaum, V. M. Gas Phase Reactions of 1,3,5-Triazine: Proton Transfer, Hydride Transfer, and Anionic σ-Adduct Formation. *J. Am. Soc. Mass Spectrom.* **2011**, *22*, 1260−1272.
(43) Moad, G.; Rizzardo, E.; Solomon, O. H. A Product Study of the Nitroxide Inhibited Thermal Polymerization of Styrene. *Polym. Bull.* **1982**, *6*, 589−593.
(44) Naik, S. S.; Savin, D. A. Poly(Z-Lysine)-Based Organogels: Effect of Interfacial Frustration on Gel Strength. *Macromolecules* **2009**, *42*, 7114−7121.
(45) Tzokova, N.; Fernyhough, C. M.; Butler, M. F.; Armes, S. P.; Ryan, A. J.; Topham, P. D.; Adams, D. J. The Effect of PEO Length on the Self-Assembly of Poly(Ethylene Oxide)-Tetrapeptide Conjugates Prepared by "Click" Chemistry. *Langmuir* **2009**, *25* (18), 11082−11089.
(46) Eckhardt, D.; Groenewolt, M.; Krause, E.; Börner, H. G. Rational Design of Oligopeptide Organizers for the Formation of Poly(Ethylene Oxide) Nanofibers. *Chem. Commun.* **2005**, 2814−2816.
(47) Dzikovski, B.; Tipikin, D.; Freed, J. Conformational Distributions and Hydrogen Bonding in Gel and Frozen Lipid Bilayers: A High Frequency Spin-Label ESR Study. *J. Phys. Chem. B* **2012**, *116*, 6694−6706.
(48) Earle, K. A.; Moscicki, J. K.; Ge, M.; Budil, D. E.; Freed, J. H. 250-GHz Electron Spin Resonance Studies of Polarity Gradients Along the Aliphatic Chains in Phospholipid Membranes. *Biophys. J.* **1994**, *66*, 1213−1221.

DOI: 10.1021/acsmacrolett.8b00728
ACS Macro Lett. 2018, 7, 1261−1266